

Published in final edited form as:

C R Phys. 2013 ; 14(6): 470–478. doi:10.1016/j.crhy.2013.04.002.

Blood viscosity in microvessels: experiment and theory

Timothy W. Secomb^a and Axel R. Pries^b

Timothy W. Secomb: secomb@u.arizona.edu

^aDepartment of Physiology, University of Arizona, Tucson, AZ 85724, USA

^bDepartment of Physiology and CCR, Charité – Universitätsmedizin Berlin, Charitéplatz 1, 10117 Berlin, Germany

Abstract

The apparent viscosity of blood flowing through narrow glass tubes decreases strongly with decreasing tube diameter over the range from about 300 μm to about 10 μm . This phenomenon, known as the Fåhræus-Lindqvist effect, occurs because blood is a concentrated suspension of deformable red blood cells with a typical dimension of about 8 μm . Most of the resistance to blood flow through the circulatory system resides in microvessels with diameters in this range. Apparent viscosity of blood in microvessels *in vivo* has been found to be significantly higher than in glass tubes with corresponding diameters. Here we review experimental observations of blood's apparent viscosity *in vitro* and *in vivo*, and progress towards a quantitative theoretical understanding of the mechanisms involved.

Keywords

capillary; microcirculation; red blood cell; rheology

1. Introduction

The relationship between the pressure generated by the heart and the resulting flow in the circulatory system has long been a subject of study. In the mid-nineteenth century, J.L.M. Poiseuille addressed this topic, and established the fourth-power dependence of flow rate Q on diameter D , for a tube with given length L and for given driving pressure p [31]. This relationship is expressed in terms of ‘Poiseuille’s law’:

$$Q = \frac{\pi}{128} \frac{\Delta p D^4}{L\mu} \quad (1)$$

where μ is the fluid viscosity. Blood, however, is a concentrated suspension of deformable cells, mainly red blood cells (RBCs), and does not exhibit a unique well-defined viscosity when it flows in narrow tubes. The resistance to flow is determined by the mechanical interactions between each RBC and the suspending medium, the tube walls, and other RBCs. The complexity of this system is evident from microscopic observations of RBCs flowing in narrow tubes, as shown in Figure 1.

Under such conditions, the effect of blood’s rheological properties on resistance to flow can be represented in terms of its apparent viscosity, which is derived from Poiseuille’s law:

$$\mu_{app} = \frac{\pi}{128} \frac{\Delta p D^4}{Q L} \quad (2)$$

For flow in a tube with given length and diameter, the resistance to blood flow (the ratio of pressure drop to flow) is directly proportional to the apparent viscosity. In general, the apparent viscosity may depend on tube diameter, flow rate, hematocrit (volume fraction of RBCs), viscosity of plasma (the suspending fluid), biophysical properties of RBCs and biophysical properties of the tube or blood vessel. The purpose of this review is to present a summary of experimental and theoretical results concerning the apparent viscosity of blood and its underlying mechanisms, and to indicate some areas of current investigation.

2. Experimental observations of apparent viscosity

2.1. Observations in vitro

Around 1930, Martini et al. [29] and Fåhræus and Lindqvist [13] observed a marked decrease in the apparent viscosity of blood in glass tubes with diameter decreasing below 300 μm , a phenomenon known as the Fåhræus-Lindqvist effect. For example, the apparent viscosity in a tube of diameter 40 μm is about 60% of its value in a 300 μm tube [13]. In subsequent years, a number of authors measured the apparent viscosity of blood in narrow glass tubes. Most of these studies used suspensions of human RBCs or whole human blood with anticoagulants. Results from several studies were assembled and reanalyzed in 1992 by Pries et al. [35, 37], who developed empirical equations to describe the dependence of relative apparent viscosity μ_{rel} (the ratio of apparent viscosity to suspending medium viscosity) on tube diameter and hematocrit:

$$\mu_{rel} = 1 + (\mu_{0.45} - 1) \frac{(1 - H_D)^C - 1}{(1 - 0.45)^C - 1} \quad (3)$$

where

$$\mu_{0.45} = 220 \exp(-1.3 D) + 3.2 - 2.44 \exp(-0.06 D^{0.645}) \quad (4)$$

and

$$C = (0.8 + \exp(-0.075 D))(-1 + (1 + 10^{-11} D^{12})^{-1}) + (1 + 10^{-11} D^{12})^{-1} \quad (5)$$

Here D is the diameter in μm and H_D is the discharge hematocrit, defined as the volume flow rate of RBCs as a fraction of the total volume flow rate. The dependence of viscosity on diameter for $H_D = 0.45$ (a typical value in humans) is given by $\mu_{0.45}$. The quantity C describes the dependence of viscosity on hematocrit, which is approximately linear for diameters up to about 8 μm but shows a highly nonlinear dependence at large diameters. In this study, only data obtained at high shear rates ($\bar{U}/D \geq 50 \text{s}^{-1}$) were considered, where \bar{U} is the mean velocity. Apparent viscosity is almost independent of flow rate in this range, but increases at lower shear rates [35, 41].

The dependence of relative apparent viscosity on diameter and discharge hematocrit, according to these equations, is illustrated in Figure 2. The trend of apparent viscosity to decrease with decreasing diameter continues down to about $7 \mu\text{m}$. At smaller diameters, relative apparent viscosity rises rapidly as the diameter approaches a critical minimum diameter, which is about $2.7 \mu\text{m}$. Although highly deformable, RBCs are subject to constraints of constant volume and almost constant surface area. These constraints prevent passage of intact cells through tubes narrower than this critical diameter.

2.2. Observations in vivo

For many years, the observed reduction of blood's apparent viscosity in narrow tubes [29, 13] was assumed to apply also to blood flow in the microvessels of living tissues. However, direct measurements *in vivo* are technically challenging due to the difficulty of measuring pressure drops in microvessels. Lipowsky et al. [27, 28] performed such measurements in vessels with diameters in the range $10\text{--}60 \mu\text{m}$ and obtained estimates of apparent viscosity substantially higher than would be expected based on the *in-vitro* behavior. The data from those experiments were not sufficiently comprehensive to establish the dependence of apparent viscosity on diameter and hematocrit.

Pries et al. [39, 40] analyzed the rheological behavior of blood in microvessels using a network-based approach. Blood flow in microvascular networks in the rat mesentery was observed experimentally and compared segment-by-segment with the predictions of theoretical models. The distributions of flow and hematocrit derived from simulations based on the parametric description of blood viscosity *in vitro* described above were found to be inconsistent with the observed behavior. However, satisfactory agreement was found when an alternative parametric description of blood viscosity was used, as follows:

$$\mu_{rel} = \left[1 + (\mu_{0.45}^* - 1) \frac{(1 - H_D)^C - 1}{(1 - 0.45)^C - 1} \left(\frac{D}{D - 1.1} \right)^2 \right] \left(\frac{D}{D - 1.1} \right)^2 \quad (6)$$

where

$$\mu_{0.45}^* = 6 \exp(-0.085 D) + 3.2 - 2.44 \exp(-0.06 D^{0.645}) \quad (7)$$

and C is given by equation (5).

The dependence of relative apparent viscosity on diameter and discharge hematocrit according to these equations is illustrated in Figure 3. The apparent viscosity decreases with decreasing diameter down to about $40 \mu\text{m}$, and rises substantially at smaller diameters. According to this result, the apparent viscosity in microvessels with diameters in the range 5 to $20 \mu\text{m}$ is much higher than expected based on the *in-vitro* results. A substantial fraction of the flow resistance in microvascular networks resides in vessels with diameters in this range. Therefore, the overall flow resistance of the microcirculation according to this relationship is expected to be significantly higher than it would be if the *in-vitro* behavior was applicable. Pries et al. [40] found that the pressure drop across mesenteric networks required to drive the observed flow rates was higher by a factor of almost 3 when the *in-vivo* behavior was assumed according to equations (6) and (7), relative to the *in-vitro* behavior, and that it

agreed well with the observed pressure drop. This and subsequent experimental findings have generally supported the conclusions described here. However, due to the above mentioned technical difficulties, systematic experimental testing of this empirically derived theory for blood's apparent viscosity *in vivo* remains to be achieved.

Possible causes for the substantial difference between apparent viscosity *in vivo* and *in vitro* were discussed by Pries et al. [39]: (i) irregularity of vessel walls; (ii) asymmetry of RBC positioning in capillaries; (iii) effects of white blood cells; (iv) retardation of plasma flow by macromolecular structures attached to vessel walls. The first three of these effects appear insufficient to account for a large part of the difference [40, 44]; see also results showing the short downstream persistence of asymmetry of cell position [50]. The main cause of the differences was shown to be the presence of a relatively thick layer, about 1 μm wide, of macromolecules bound to the endothelial cells lining microvessel walls, known as the glycocalyx or endothelial surface layer (ESL) [38]. Indeed, a subsequent theoretical model [36], which includes an ESL whose effective thickness depends on both vessel diameter and hematocrit, leads to closer agreement between theoretical predictions of network hemodynamics and observed behavior, relative to the model described by equations (6)–(7). In this model, the apparent viscosity is again substantially increased relative to *in-vitro* behavior, but the dependence on diameter is more complicated, with a peak at about 10 μm .

3. Theoretical analysis of blood flow in narrow tubes

3.1. Mechanical properties of red blood cells

Blood is a suspension of cells in plasma, which is an incompressible Newtonian fluid with a viscosity of about 1 cP. The cells are RBCs (erythrocytes), white blood cells (leukocytes) of several different types, and platelets. The hematocrit of normal human blood is 40–45%, and RBCs consequently have a dominant effect on the flow properties of blood. The key mechanical properties of human RBCs were established more than 30 years ago, including quantitative estimates of key mechanical parameters [52, 10, 11]. This information has provided a basis for developing detailed theoretical models for the behavior of blood and suspensions of RBCs in various flow geometries, including narrow tubes, as described below.

Human (and other mammalian) RBCs are notable for their high degree of deformability, which is a consequence of their structure. Lacking a nucleus, they consist of a fluid interior surrounded by a thin membrane. The membrane consists of two main components: the lipid bilayer and the cytoskeleton. The lipid bilayer behaves as an almost incompressible two-dimensional fluid, and the cell therefore strongly resists area changes, with an elastic modulus of isotropic dilation of about 500 dyn/cm. The cytoskeleton, a network of protein molecules, lies immediately inside the lipid bilayer, and has components that project into the bilayer, coupling the two structures. Even so, the bilayer and the cytoskeleton can move relative to each other, as for instance when part of the membrane is stretched into a narrow tongue [8].

The membrane has a relatively small resistance to bending, with a bending modulus of about 1.8×10^{-12} dyn-cm [12]. Bending moments in the membrane become important only in

regions of the membrane where its radius of curvature is very small. The membrane also possesses a viscous resistance to transient in-plane shear deformations. This resistance is generated mainly in the cytoskeleton, with a small contribution from membrane viscosity [10]. The viscoelastic behavior of the membrane in shear can be represented by a Kelvin solid model. According to this model, the total shear stress is represented as the sum of viscous and elastic contributions [10]. The cell's interior consists of a concentrated solution of the oxygen-binding protein hemoglobin and behaves as a viscous incompressible fluid.

3.2. Theoretical analysis of capillary flow

In capillaries with diameters up to about $8\ \mu\text{m}$, RBCs frequently flow in single file. Interactions between cells may then be negligible and theoretical analysis of a single RBC is appropriate. In such vessels, RBCs are compressed into narrow bullet-like shapes, and their mechanics can be analyzed by assuming that the RBC has rotational symmetry about the tube axis. A further simplification is the use of lubrication theory to describe the motion of the suspending fluid in the space between the cell and the vessel wall. This approach was developed by several authors, starting in 1968 [2, 26, 62, 49, 41]. The key elements of the approach are as follows: (i) the axisymmetric cell shape is described in cylindrical polar coordinates $(r(s), \theta, z(s))$ where s is arc length measured along the membrane from the front of the cell in the plane $z = 0$; (ii) the components of membrane tension and bending moments are expressed in terms of stretch ratios and curvatures in the axial and circumferential directions; (iii) the fluid loading on the cell is computed using axisymmetric lubrication theory to describe the flow field in the gap between the cell and the vessel wall; (iv) the resulting system of ordinary differential equations and boundary conditions is solved numerically to predict cell shapes and apparent viscosity [49]. Figure 4 shows cell shapes computed by this method. Predicted shapes are consistent with experimental observations in glass tubes [18, 54] and with subsequent theoretical simulations using a boundary-integral method [32]. The corresponding estimates of apparent viscosity show good quantitative agreement with experimental findings as a function of both cell velocity and tube diameter up to $8\ \mu\text{m}$ [41, 43], as indicated in figure 5. The low values of relative apparent viscosity for diameters in the range 5 to $8\ \mu\text{m}$ arise because the highly deformed shapes of the RBCs allow the formation of a cell-free layer surrounding the cells, which lubricates their motion.

In reality, the shapes of RBCs flowing in capillaries are not generally axisymmetric. In narrow capillaries, the front part of the cell typically assumes a nearly axisymmetric bullet shape, but the rear edge of the cell is obliquely oriented, as illustrated in Figure 1. Analysis of the motion of cells with such shapes shows that the effect of asymmetry on apparent viscosity is small [22]. This analysis includes the effect of continuous 'tank-treading' motion of the membrane around the cell driven by the asymmetric fluid loading. More recently, the motion of RBCs that enter a capillary in an asymmetric position was simulated using a simplified 2D model of RBC mechanics [50]. It was found that the cells migrate to the center-line within a few tens of μm . Predicted cell trajectories agreed closely with experimental observations in capillaries of the rat mesentery.

Several studies have examined the motion of RBCs in capillaries, considering the effects of the ESL [6, 45, 15]. It was shown [45] that an ESL with a thickness of about $1\ \mu\text{m}$, acting as

a porous medium with hydraulic resistivity of at least 10^8 dyn-s/cm⁴, led to predicted values of apparent viscosity in a 6- μ m capillary consistent with the *in-vivo* findings as already described. A notable finding was that a moving RBC can ride on the surface of the ESL, under conditions where a static RBC would expand to fill the entire lumen, compressing the ESL [15, 47].

The functional significance of the ESL has not been definitely established. A structure that increases flow resistance might be thought to be detrimental to blood flow, but this effect can be compensated for by a small increase in vessel diameters. The ESL has been shown to modulate the access of cells and macromolecules to the endothelial cell membrane [56, 57], and its effects on the environment experienced by endothelial cells may be important. Shear stress resulting from blood flow has been shown to be transmitted to the endothelial cells primarily via the attachment points of the glycocalyx, not as fluid shear stress [46]. The mechanism by which shear stress is transmitted within the ESL has been the subject of debate. Pries et al. [38] proposed that membrane-bound chain structures, under tension as a result of osmotic swelling, carry the shear stress, whereas Weinbaum et al. [59] considered that filaments in the layer act as cantilever beams. Independent of the mechanism, the ESL may have a significant effect on the mechanotransduction of shear stress into biological signals. In reality, capillaries have irregular cross-sections, as a result for example of endothelial cell nuclei that project into the vessel lumen. The ESL may help to shield RBCs from mechanical damage during the many transits that each cell makes through the circulatory system during its approximately 120-day lifetime [48].

3.3. Models of multi-file flow

In tubes with diameters of 7–8 μ m or more, RBCs may exhibit multi-file flow, depending on the hematocrit [18]. As in the case of single-file flow, the low values of apparent viscosity observed in multi-file flow result primarily from the presence of a cell-free or cell-depleted layer adjacent to the vessel wall. The effect of such a layer on apparent viscosity (in the absence of an ESL) can be illustrated by considering a simple two-layer model (the modified axial-train model), in which the RBCs are contained within a cylindrical core region of diameter λD that is concentric with the tube and has a uniform viscosity μ_{core} and the surrounding cell-free annular wall layer has viscosity μ_p . The apparent viscosity is then [55]:

$$\mu_{app} = \frac{\mu_p}{1 - \lambda^4(1 - \mu_p/\mu_{core})}. \quad (8)$$

A relatively narrow plasma layer (λ slightly less than one) can have a substantial impact on apparent viscosity, because it decreases the local viscosity in the region near the wall where viscous energy dissipation would otherwise be concentrated. For tube diameters above 30 μ m, equation (8) gives a good fit to experimental results assuming $\mu_{core}/\mu_p = 3.3$ and a fixed cell-free layer width of 1.8 μ m [42], as shown in Figure 5.

Simulation of the flow of multiple interacting flexible particles in three dimensions is a challenging computational task. During the last several years, increases in computer power and development of lattice-based and particle-based methods have made such computations possible [30, 9, 14]. Simulations of flow at physiological hematocrits in vessels with

diameters in the range 10 to 40 μm have led to estimates of apparent viscosities close to those of *in-vitro* experiments [9, 14]. The predicted mean cell-free layer thickness at hematocrit 0.45 in tubes with diameters 20 and 40 μm was close to 1.8 μm , in agreement with the empirical estimate mentioned above [14]. These techniques have demonstrated the ability to predict quantitatively the flow properties of blood in microvessels with diameters up to about 40 μm , and represent a substantial advance. In principle, they allow simulation of multi-file blood flow in any well-characterized microvascular geometry, although the computational cost increases at least in proportion to the number of RBCs in the domain.

Despite the success of these simulations, the principles governing multi-file flow of RBCs remain incompletely understood. Ideally, a quantitative theory of such flows would provide a basis for predicting the evolution of the hematocrit profile along a flowing microvessel, without the need to simulate the motion of every individual RBC. It would also describe the relationship between pressure gradient and flow rate at each axial position. This information could be used for efficient simulation of flow and RBC flux distributions in entire microvascular networks, taking into account the variations of hematocrit and velocity profiles resulting from bifurcations and other irregularities. Such simulations are not feasible with currently available methods.

Previous studies provide a conceptual basis for understanding the key processes that govern the distribution of interacting deformable particles flowing in narrow channels. Two competing mechanisms are involved [43, 33]: a tendency to migrate away from the walls [19, 23], and ‘shear-induced diffusion’ down the concentration gradient toward the wall, resulting from particle-particle interactions [24]. The tendency to migrate away from the walls has two causes [5]: a lift force induced by the interaction of the particles flow field with the solid boundary, and the non-constant shear rate in a parabolic velocity profile. The strength of particle-particle interactions is dependent on hematocrit, and the cell-free layer thickness consequently decreases with increasing hematocrit, as observed both experimentally and in simulations [4, 14].

Considering a suspension of elastic capsules, Pranay et al. [33] recently derived a closed-form expression for the width of the particle-depleted layer, and showed that it varies inversely with particle concentration. This result is significant in that it represents in a quantitative form the dependence of the layer width on the balance between particle migration away from the walls and shear-induced diffusion. However, it has some limitations with regard to the prediction of cell-depleted layer thickness in microvessels. The expression [33] involves a number of coefficients that depend on the deformability, shape and orientation of the particles. These coefficients are not explicitly known for RBCs, and likely depend on hematocrit and on shear rate. In this theory, the estimation of the migration of particles from the wall is based on a consideration of the particle as a point dipole. This is appropriate when the particle is not very close to the wall. However, at physiological hematocrits, the distance of RBCs from the wall (about 2 μm) is typically much less than the particle size (about 8 μm). In such cases, the forces driving cells away from the wall may be highly sensitive to the shape of the RBC in regions where it is closest to the wall. The theory for generation of lift forces on deformable particles close to solid boundaries according to

lubrication theory [53] may be helpful in obtaining insight into the relationship between the deformation of RBCs that approach the walls and the resulting generation of lift forces [20].

With regard to multi-file flow, the effects of interactions between flowing RBCs and the endothelial surface layer have received little attention. Two studies have examined the effect of such a layer on migration of individual particles near a vessel wall, subject to a shear flow. Beaucourt et al. [3] modeled the interactions of rigid and deformable vesicles with a compressible but impermeable wall substrate, representing the ESL. Conversely, Hariprasad and Secomb [20] considered the layer to be permeable but of fixed width, and showed that the rate of lateral migration of two-dimensional model RBCs decreased with increasing permeability of the layer.

4. RBC motion in microfluidic systems

In recent years, the ability to fabricate microfluidic systems using photolithographic methods has opened new possibilities for manipulating and studying blood flow in microscale geometries [60]. The potential of such approaches for investigating normal and pathological behavior of blood cells and for developing new diagnostic and therapeutic approaches is currently being explored. Here, a few examples will be cited. With regard to the resistance of microvessels to blood flow, microfluidic systems can be used to detect the changes in flow resistance associated with the passage of individual red and white blood cells through a narrow channel [1]. The effects on RBC deformation of chemically modifying the cells' mechanical properties can be assessed by observing shape changes of individual cells when they traverse a channel with a microfluidic constriction [16]. Similarly, such techniques can be used to explore the consequences for microvascular blood flow of diseases in which RBCs exhibit abnormal mechanical properties, including malaria [51] and sickle cell disease [21]. RBCs are known to release ATP (adenosine triphosphate), a substance that participates in control of blood flow by modulating vessel diameters [7]. Cell deformation is one of the factors affecting the rate of ATP release, and this phenomenon can be examined on cellular scales using microfluidic systems [58, 17]. The non-uniform partition of suspended RBCs in diverging vessel bifurcations [34] provides a basis for separating RBCs from plasma or sorting them according to their properties in microfluidic systems, with potential diagnostic or therapeutic applications [61, 25]. These experimental approaches, in combination with newer computational approaches as described above, have led to an upsurge of research activity on the microscale flow properties of blood.

5. Conclusions

Despite many decades of investigation, understanding the relationship between pressure gradient and blood flow rate in microvessels has remained an elusive goal. Classic experiments using glass tubes [29, 13] revealed a striking reduction in apparent viscosity at small diameters, the Fåhræus-Lindqvist effect, and a consistent set of data for apparent viscosity as a function of diameter and hematocrit was subsequently developed [35]. Theoretical studies based on the known mechanical properties of RBCs led to successful quantitative prediction of apparent viscosity in single-file flow about 25 years ago [41], while corresponding results for multi-file flow in diameters up to 40 μm were achieved only

recently [9, 14]. Direct tests of these theories by experimental measurement of pressure drops in individual microvessels is technically very difficult. Eventually, an indirect approach based on examining network flows showed that microvessel apparent blood viscosity *in vivo* is substantially higher than in corresponding glass tubes [40], with the difference being mainly attributable to a hemodynamically significant ESL.

The mechanical properties of human and mammalian RBCs have been studied in detail and are well characterized at a quantitative level. This information provides a good basis for theoretical simulation of blood flow in a variety of conditions. For single-file flow in capillary-sized vessels, such simulations yield predictions of apparent viscosity that agree well with observations in glass tubes. The substantial difference between apparent viscosity *in vitro* and *in vivo* can be accounted for by the inclusion of a porous layer representing the ESL. Recently, powerful numerical techniques have been applied to three-dimensional simulation of multiple interacting RBCs, leading to quantitative prediction of apparent viscosity. However, a number of theoretical challenges remain with regard to the multi-file flow of RBCs. Firstly, the phenomenon of shear-induced diffusion is not well understood for concentrated suspensions of highly deformable particles, including RBCs. Here, it is important to distinguish between the random migration of individual particles and the evolution of the concentration profile, which depends on net particle migration. Secondly, while the mechanisms responsible for the migration of deformable particles away from solid boundaries are understood in principle, quantitative theories applicable to RBCs very close to boundaries are not available. Thirdly, the interaction between the ESL and RBCs in multi-file flow remains to be investigated. Experimental evidence [36] suggests that this interaction is strongly diameter-dependent. Progress in all these areas is needed in order to achieve a good understanding of the mechanisms determining the apparent viscosity of blood in microvessels.

Acknowledgments

This work was supported by NIH Grant HL034555.

References

1. Abkarian M, Faivre M, Stone HA. Proc Natl Acad Sci USA. 2006; 103:538–542. [PubMed: 16407104]
2. Barnard ACL, Lopez L, Hellums JD. Microvasc Res. 1968; 1:23–34.
3. Beaucourt J, Biben T, Misbah C. Europhysics Letters. 2004; 67:676–682.
4. Bugliarello G, Sevilla J. Biorheology. 1970; 7:85–107. [PubMed: 5484335]
5. Coupier G, Kaoui B, Podgorski T, Misbah C. Physics of Fluids. 2008; 20:111702.
6. Damiano ER. Microvasc Res. 1998; 55:77–91. [PubMed: 9473411]
7. Dietrich HH, Ellsworth ML, Sprague RS, Dacey RG Jr. Am J Physiol Heart Circ Physiol. 2000; 278:H1294–H1298. [PubMed: 10749727]
8. Discher DE, Mohandas N, Evans EA. Science. 1994; 266:1032–1035. [PubMed: 7973655]
9. Doddi SK, Bagchi P. Physical Review E. 2009; 79:046318.
10. Evans EA, Hochmuth RM. Biophys J. 1976; 16:1–11. [PubMed: 1244886]
11. Evans, EA.; Skalak, R. Mechanics and Thermodynamics of Biomembranes. CRC Press; Boca Raton, Florida: 1980.
12. Evans EA. Biophys J. 1983; 43:27–30. [PubMed: 6882860]

13. Fåhræus R, Lindqvist T. *Am J Physiol.* 1931; 96:562–568.
14. Fedosov DA, Caswell B, Popel AS, Karniadakis GE. *Microcirculation.* 2010; 17:615–628. [PubMed: 21044216]
15. Feng J, Weinbaum S. *Journal of Fluid Mechanics.* 2000; 422:281–317.
16. Forsyth AM, Wan J, Ristenpart WD, Stone HA. *Microvasc Res.* 2010; 80:37–43. [PubMed: 20303993]
17. Forsyth AM, Wan J, Owrutsky PD, Abkarian M, Stone HA. *Proc Natl Acad Sci USA.* 2011; 108:10986–10991. [PubMed: 21690355]
18. Gaetgens P, Dührssen C, Albrecht KH. *Blood Cells.* 1980; 6:799–812. [PubMed: 7470632]
19. Goldsmith HL. *Fed Proc.* 1971; 30:1578–1590. [PubMed: 5119364]
20. Hariprasad DS, Secomb TW. *Journal of Fluid Mechanics.* 2012; 705:195–212. [PubMed: 23493820]
21. Higgins JM, Eddington DT, Bhatia SN, Mahadevan L. *Proc Natl Acad Sci USA.* 2007; 104:20496–20500. [PubMed: 18077341]
22. Hsu R, Secomb TW. *J Biomech Eng.* 1989; 111:147–151. [PubMed: 2733409]
23. Leal LG. *Ann Rev Fluid Mech.* 1980; 12:435–476.
24. Leighton D, Acrivos A. *Journal of Fluid Mechanics.* 1987; 181:415–439.
25. Li X, Popel AS, Karniadakis GE. *Phys Biol.* 2012; 9:026010. [PubMed: 22476709]
26. Lighthill MJ. *Journal of Fluid Mechanics.* 1968; 34:113–143.
27. Lipowsky HH, Kovalcheck S, Zweifach BW. *Circ Res.* 1978; 43:738–749. [PubMed: 709740]
28. Lipowsky HH, Usami S, Chien S. *Microvasc Res.* 1980; 19:297–319. [PubMed: 7382851]
29. Martini P, Pierach A, Schreyer E. *Dt Arch Klin Med.* 1930; 169:212–222.
30. McWhirter JL, Noguchi H, Gompper G. *Proc Natl Acad Sci USA.* 2009; 106:6039–6043. [PubMed: 19369212]
31. Poiseuille JLM. *Mémoires présentés par divers savants à l'Académie Royale des Sciences de l'Institut de France.* 1846; IX:433–544.
32. Pozrikidis C. *Physics of Fluids.* 2005; 17:031503.
33. Pranay P, Henríquez-Rivera RG, Graham MD. *Physics of Fluids.* 2012; 24:061902.
34. Pries AR, Ley K, Claassen M, Gaetgens P. *Microvasc Res.* 1989; 38:81–101. [PubMed: 2761434]
35. Pries AR, Neuhaus D, Gaetgens P. *Am J Physiol.* 1992; 263:H1770–H1778. [PubMed: 1481902]
36. Pries AR, Secomb TW. *Am J Physiol Heart Circ Physiol.* 2005; 289:H2657–H2664. [PubMed: 16040719]
37. Pries, AR.; Secomb, TW. *Handbook of Physiology: Microcirculation.* Second. Tuma, RF.; Duran, WN.; Ley, K., editors. Academic Press; San Diego: 2008. p. 3-36.
38. Pries AR, Secomb TW, Gaetgens P. *Pflügers Arch.* 2000; 440:653–666. [PubMed: 11007304]
39. Pries AR, Secomb TW, Gaetgens P, Gross JF. *Circ Res.* 1990; 67:826–834. [PubMed: 2208609]
40. Pries AR, Secomb TW, Gessner T, Sperandio MB, Gross JF, Gaetgens P. *Circ Res.* 1994; 75:904–915. [PubMed: 7923637]
41. Secomb TW. *Microvasc Res.* 1987; 34:46–58. [PubMed: 3657604]
42. Secomb TW. *Symp Soc Exp Biol.* 1995; 49:305–321. [PubMed: 8571232]
43. Secomb, TW. *Hydrodynamics of Capsules and Cells.* Pozrikidis, C., editor. Chapman & Hall/CRC; Boca Raton, Florida: 2003. p. 163-196.
44. Secomb TW, Hsu R. *Microcirculation.* 1997; 4:421–427. [PubMed: 9431510]
45. Secomb TW, Hsu R, Pries AR. *Am J Physiol.* 1998; 274:H1016–H1022. [PubMed: 9530216]
46. Secomb TW, Hsu R, Pries AR. *Biorheology.* 2001; 38:143–150. [PubMed: 11381171]
47. Secomb TW, Hsu R, Pries AR. *Am J Physiol Heart Circ Physiol.* 2001; 281:H629–H636. [PubMed: 11454566]
48. Secomb TW, Hsu R, Pries AR. *Microcirculation.* 2002; 9:189–196. [PubMed: 12080416]
49. Secomb TW, Skalak R, Özkaya N, Gross JF. *Journal of Fluid Mechanics.* 1986; 163:405–423.
50. Secomb TW, Styp-Rekowska B, Pries AR. *Ann Biomed Eng.* 2007; 35:755–765. [PubMed: 17380392]

51. Shelby JP, White J, Ganesan K, Rathod PK, Chiu DT. Proc Natl Acad Sci USA. 2003; 100:14618–14622. [PubMed: 14638939]
52. Skalak, R. Microcirculation, Vol I, Plenum. Grayson, J.; Zingg, W., editors. New York: 1976. p. 53-70.
53. Skotheim JM, Mahadevan L. Physics of Fluids. 2005; 17:092101.
54. Tomaiuolo G, Simeone M, Martinelli V, Rotoli B, Guido S. Soft Matter. 2009; 5:3736–3740.
55. Vand V. J Phys Colloid Chem. 1948; 52:277–299. [PubMed: 18906401]
56. Vink H, Duling BR. Circ Res. 1996; 79:581–589. [PubMed: 8781491]
57. Vink H, Duling BR. Am J Physiol Heart Circ Physiol. 2000; 278:H285–H289. [PubMed: 10644610]
58. Wan J, Forsyth AM, Stone HA. Integr Biol (Camb). 2011; 3:972–981. [PubMed: 21935538]
59. Weinbaum S, Zhang X, Han Y, Vink H, Cowin SC. Proc Natl Acad Sci USA. 2003; 100:7988–7995. [PubMed: 12810946]
60. Wong KH, Chan JM, Kamm RD, Tien J. Annu Rev Biomed Eng. 2012; 14:205–230. [PubMed: 22540941]
61. Yang S, Undar A, Zahn JD. Lab Chip. 2006; 6:871–880. [PubMed: 16804591]
62. Zarda, PR.; Chien, S.; Skalak, R. Computational Methods for Fluid-Solid Interaction Problems. Belytschko, T.; Geers, TL., editors. American Society of Mechanical Engineers; New York: 1977. p. 65-82.

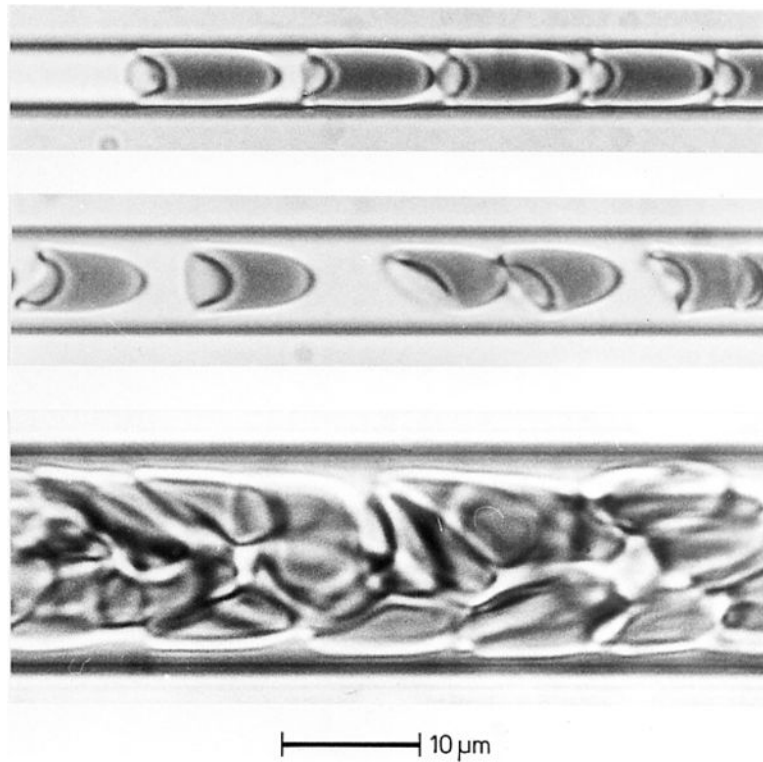


Figure 1. Human RBCs flowing in glass tubes of approximate diameters $4.5 \mu\text{m}$ (top), $7 \mu\text{m}$ (middle), and $15 \mu\text{m}$ (bottom). The flow direction is from left to right. Reproduced from [43] by permission.

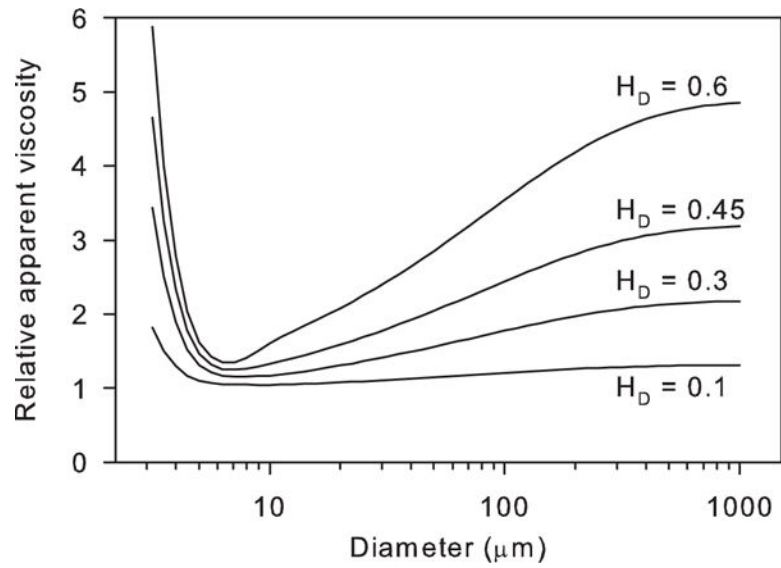


Figure 2. Dependence of relative apparent viscosity of blood in glass tubes on diameter, for different levels of discharge hematocrit, according to the empirical equations (3)–(5).

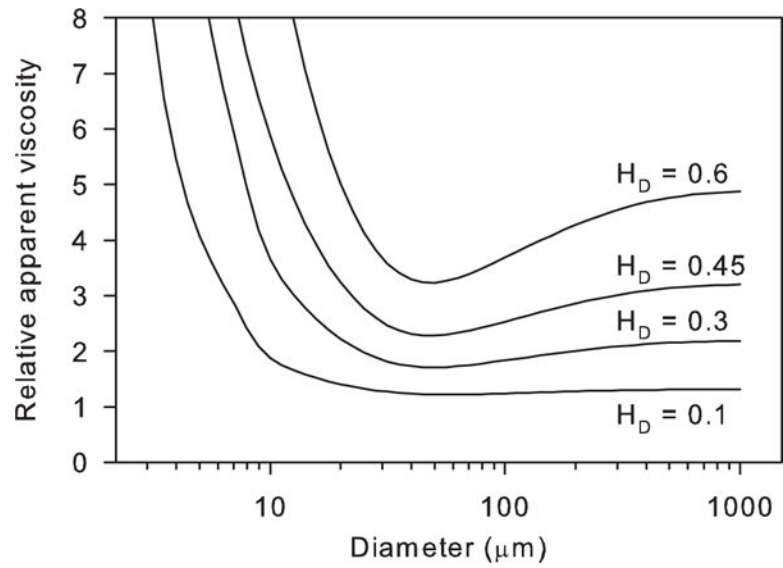


Figure 3. Dependence of relative apparent viscosity of blood in glass tubes on diameter, for different levels of discharge hematocrit, according to the empirical equations (6)–(7).

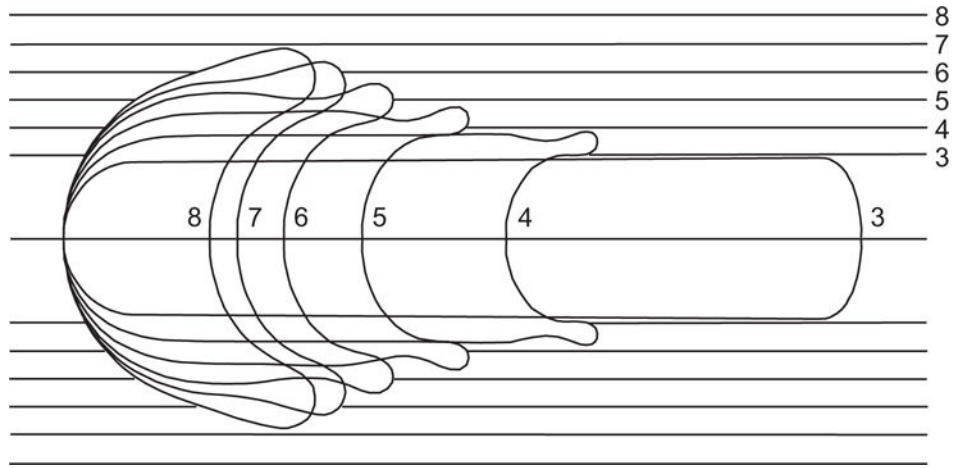


Figure 4. Computed axisymmetric red blood cell shapes, for tube diameters in μm as indicated. Flow is from right to left with velocity 0.01 cm/s. Results redrawn after [43].

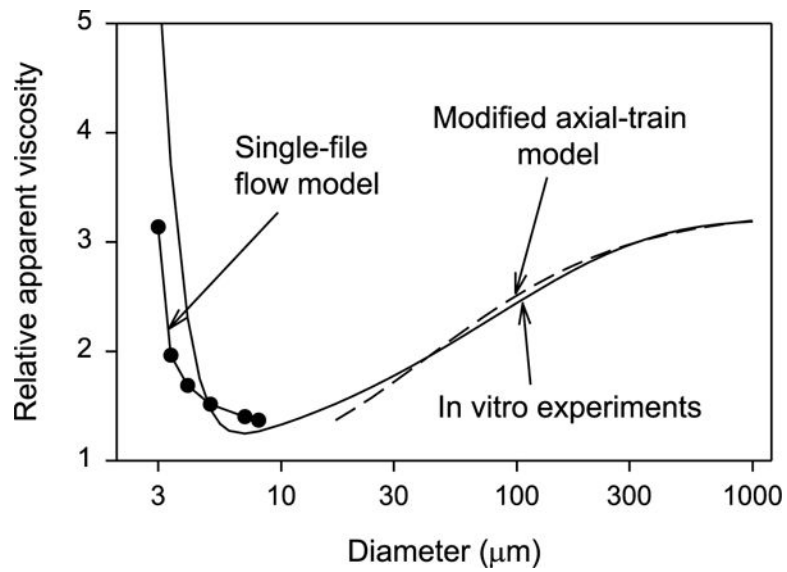


Figure 5. Variation of relative apparent viscosity with tube diameter, for a discharge hematocrit of 45%, and for relatively high flow rates. Solid curve: empirical fit to experimental in vitro data [35]. Solid circles: numerical results, obtained using an approximate analysis for the high-velocity limit [49, 41]. Dashed curve: modified axial-train model, with $\mu_{core}/\mu_p = 3.3$ and cell-free layer width = $1.8 \mu\text{m}$. Reproduced from [43] by permission.